

Temporal evolution of the electron energy distribution function in oxygen and chlorine gases under dc and ac fields

Ping Jiang and Demetre J. Economou^{a)}

Plasma Processing Laboratory, Department of Chemical Engineering, University of Houston, Houston, Texas 77204-4792

(Received 25 November 1992; accepted for publication 19 February 1993)

An analysis of the temporal evolution of the electron energy distribution function (EEDF) and the electron swarm parameters in oxygen and chlorine gases is presented. The spatially homogeneous time-dependent Boltzmann equation is solved for dc and radio-frequency ac electric fields by a finite-element method. A comparison is made of the swarm parameters obtained for the following three cases: (a) under the actual ac field; (b) assuming that the EEDF follows faithfully the applied ac field [quasi-steady-state (QSS) approximation]; and (c) using an "effective" dc field (effective dc approximation). It is shown that the effective dc approximation is not applicable to either oxygen or chlorine for frequencies < 10 MHz; however, the QSS approximation is justified for chlorine discharges at < 13.56 MHz. This has important implications for reducing the computation time in modeling the bulk plasma of glow discharge reactors. It is also shown that atomic chlorine resulting from molecular dissociation has a significant effect on the swarm parameters, especially for large degrees of gas dissociation.

I. INTRODUCTION

Low-pressure molecular gas discharges are used widely in materials processing, gas lasers, and other applications.^{1,2} Electron-impact reactions with gas species are of primary importance in these discharges. For example, electron-impact molecular dissociation yields radicals and other reactive intermediates which are responsible for much of the chemistry taking place in glow discharges. Knowledge of the electron velocity distribution function and derived quantities (electron transport and rate coefficients) is essential for studying kinetics and transport in glow discharge processes. The electron velocity distribution function can be obtained by solving the Boltzmann transport equation.³ Quite often the electron drift velocity is much smaller than the electron thermal velocity. In such a case, the isotropic part of the distribution function is dominant. The electron energy distribution function (EEDF) can be derived from the velocity distribution function by using the relationship between velocity and energy.²

A number of investigators have studied the steady-state EEDF in various gas discharges under an applied dc electric field. For example, Engelhardt and Phelps⁴ derived a set of elastic and inelastic collision cross sections for electrons in H₂ and D₂ by solving the Boltzmann equation using the two-term approximation. Nighan⁵ studied the EEDF and collision rates in N₂, CO, and CO₂ gases. Tagashira, Sakai, and Sakamoto⁶ solved the Boltzmann equation for high reduced electric fields (E/N) in Ar. Yachi *et al.*⁷ used a multiterm approximation to solve the Boltzmann equation for CH₄.

When the applied electric field varies with time, the

EEDF is correspondingly time dependent. For sufficiently high frequencies of the ac field, calculation of the EEDF is greatly simplified by introducing the effective dc field approximation.⁸⁻¹⁰ In this approximation, the actual ac field is replaced by an effective dc field which presumably transfers the same energy to the electrons. Although the effective dc approximation has been used widely, there is uncertainty as to under which conditions this approximation is valid. On the other hand, for sufficiently low frequencies, one may assume that the EEDF follows the applied field in a quasi-steady-state manner, i.e., at any particular point in time the EEDF would be identical to that calculated for a dc field of the same strength as that of the ac field at that point in time. The quasi-steady-state (QSS) approximation was recently used for modeling rf chlorine plasmas sustained between parallel plates^{11,12} and in tubular reactors.¹³ Both the effective dc and QSS approximations afford considerable savings in computation time since, under these approximations, the time-dependent Boltzmann equation does not need to be solved.

The "high-" and "low-" frequency limits can be estimated by knowing the electron energy relaxation frequency (ν_u). When the angular frequency of the applied field $\omega \ll \nu_u$, the characteristic time for energy relaxation is much shorter than the period of the applied field. As a consequence, the EEDF can follow the time variation of the applied field in a quasistationary manner. At the other extreme of $\omega \gg \nu_u$, the EEDF cannot follow the variation of the field, and the EEDF attains a nearly time-independent state. However, many practical rf discharges excited in the 1–100 MHz range fall in the intermediate regime of applied frequencies (say, for $0.1 < \omega/\nu_u < 10$). The situation is further complicated by realizing that ν_u is a function of electron energy. Hence, the condition $\omega < \nu_u$ may be realized for the tail of the distribution, while the opposite ($\omega > \nu_u$)

^{a)} Author to whom correspondence should be addressed.

is true for the low-energy part of the distribution. Under these conditions it is not clear whether the effective dc or QSS approximations can be applied, or what error in the computed electron transport and reaction coefficients will result by applying any of the two approximations. In order to resolve this issue, one needs to solve the time-dependent Boltzmann equation and compare the results with those of the approximate solutions. If any of the approximations can be applied the computation time can be reduced significantly.

Recently, the time modulation of the EEDF under an applied rf field has been studied both experimentally^{14,15} and theoretically.¹⁶⁻¹⁸ Makabe and Goto¹⁶ demonstrated that it is necessary to consider the time dependence of the electron distribution function even at high-frequency fields for molecular gases that exhibit a Ramsauer minimum. Capitelli *et al.*¹⁷ reported a calculation of the time modulation of the EEDF in SiH₄ and SiH₄-H₂ gases under a rf field. Feoktistov *et al.*¹⁸ considered the space- and time-dependent Boltzmann equation in He gas as part of a glow discharge model for a parallel-plate rf plasma reactor. However, the temporal evolution of the EEDF in oxygen or chlorine gases under rf field excitation has not been reported.

The temporal evolution of the EEDF is also important during plasma ignition or extinction. For example, pulsed plasmas are used for minimizing particulates in SiH₄ plasma deposition discharges,¹⁹ for the study of plasma and radical kinetics,²⁰ as well as for a variety of other applications. As the EEDF cools down during the plasma off period of the cycle, rapid electron attachment to electronegative species can create a large concentration of negative ions which have a strong influence on the discharge characteristics and in turn on the quality of the deposited film. The EEDF and corresponding swarm parameter transient can be studied by imposing step changes on the electric field and observing the response.²¹

In this work, the spatially uniform time-dependent Boltzmann transport equation is solved for the electron energy distribution function in oxygen and chlorine gases in the 1–100 MHz frequency range, for conditions typical of low-pressure (~1 Torr) discharges used for materials processing. Electron transport and reaction coefficients are calculated as a function of time for (a) step changes in the electric field to determine time constants for EEDF equilibration as well as the temporal evolution of radical production rate coefficients, and (b) radio-frequency sinusoidal electric fields to study the degree of modulation of the electron swarm parameters, and to test the applicability of the effective dc and QSS approximations.

II. THEORETICAL DEVELOPMENT

A. Model formulation

1. Boltzmann equation

The general form of the Boltzmann equation is²

$$\left(\frac{\partial}{\partial t} + \mathbf{v} \cdot \nabla_{\mathbf{r}} + \frac{\mathbf{F}}{m} \cdot \nabla_{\mathbf{v}} \right) f(\mathbf{r}, \mathbf{v}, t) = S = \left(\frac{\delta f}{\delta t} \right)_{\text{coll}}, \quad (1)$$

where $f(\mathbf{r}, \mathbf{v}, t)$ is the electron velocity distribution function (EVDF) at time t and spatial location \mathbf{r} . Here \mathbf{v} is the electron velocity and $S = (\delta f / \delta t)_{\text{coll}}$ is the collision integral which depends upon the details of the collision processes electrons undergo. In order to streamline the computational effort, the following simplifications were made.

(i) $f = f(\mathbf{v}, t)$, i.e., f is uniform in space. This implies that there are no spatial gradients of the electric field or electron density.

(ii) The following also holds:

$$f(\mathbf{v}, t) \approx f_0(v, t) + (\mathbf{v}/v) \cdot \mathbf{f}_1(v, t),$$

i.e., a first-order spherical harmonic expansion of the EVDF is employed.³⁻⁸ Here f_0 is the isotropic part of the distribution and \mathbf{f}_1 is the anisotropic part. This so-called Lorenz approximation is quite popular and has been found to be adequate for a wide range of gases²² when (a) the electric field to neutral density ratio E/N is relatively small, and (b) the elastic collision cross section is much higher than the inelastic collision cross sections. When accounting for production of secondary electrons by ionization, the two-term expansion may be applicable even for strong fields.²³ In fact the two-term expansion has been used extensively to derive consistent sets of collision cross sections.⁴ When using sets of cross sections derived this way, the two-term expansion may give more accurate results than a multiterm expansion; however, the two-term approximation may be poor when anisotropic electron transport is important. An example is the sheath region of low-frequency (< 10 MHz) discharges in which secondary electrons emitted from the wall accelerate in the sheath forming an electron beam.

(iii) For ac frequencies less than the momentum exchange frequency, $\mathbf{f}_1(v, t)$ follows faithfully the applied field. Then $\mathbf{f}_1(v, t)$ can be assumed to be in quasisteady state with the field and

$$\mathbf{f}_1(v, t) = - \left(\frac{\mathbf{F}}{[m\nu_m(v)]} \right) \frac{\partial f_0(v, t)}{\partial v},$$

$\nu_m(v)$ being the electron momentum exchange frequency. The quasi-steady-state approximation for $\mathbf{f}_1(v, t)$ is applicable for the frequency range examined in this work, namely 1–100 MHz.

(iv) $\mathbf{F} = q\mathbf{E}$, where q is electric charge ($-e$ for an electron) and \mathbf{E} is the dc or ac electric field applied. No magnetic-field effects are considered.⁸

(v) Temporal variations of electron density do not affect the shape of the distribution function. This assumption is reasonable even in ac discharges since electron density modulation in the bulk plasma is rather weak.²⁴

(vi) Inelastic collisions of the first kind (ionization, excitation) are more important than collisions of the second kind. Therefore, processes such as superelastic electron collisions with metastable oxygen molecules are neglected. Electron-electron collisions are also neglected.

Under these assumptions and after converting velocity to energy ($\epsilon = mv^2/2$), the Boltzmann equation can be written as (in the following f is used instead of f_0 for simplicity)

$$\sqrt{\epsilon} \frac{\partial f}{\partial t} = -\frac{\partial J_\epsilon}{\partial \epsilon} + N[Q_{el}(f) + Q_{in}(f)], \quad (2)$$

where J_ϵ is a flux in the energy coordinate

$$J_\epsilon = -\frac{1}{3} \left(\frac{2}{m}\right)^{1/2} \left(\frac{eE}{N}\right)^2 \frac{\epsilon}{\sum_k y_k \sigma_{mk}(\epsilon)} N \left(\frac{\partial f}{\partial \epsilon}\right). \quad (3)$$

N is the gas number density and $Q_{el}(f)$, $Q_{in}(f)$ are the elastic and inelastic collision integrals, respectively, which are given by

$$Q_{el}(f) = \sqrt{8m} \frac{\partial}{\partial \epsilon} \left[\left(\frac{\sum_k y_k \sigma_{mk}(\epsilon)}{M_k} \right) \epsilon^2 \left(f + kT_g \frac{\partial f}{\partial \epsilon} \right) \right], \quad (4)$$

$$Q_{in}(f) = \left(\frac{2}{m}\right)^{1/2} \sum_k y_k \sum_j [(\epsilon + I_{jk}) \sigma_{jk}(\epsilon + I_{jk}) \times f(\epsilon + I_{jk}, t) - \epsilon \sigma_{jk}(\epsilon) f(\epsilon, t)] + Q_{att}(f) + Q_{rot}(f). \quad (5)$$

Here, $Q_{att}(f)$ and $Q_{rot}(f)$ are the collision integrals for attachment and rotational excitation, respectively. In the above summations, index k runs over all heavy species and index j runs over all inelastic electron collisions, excluding attachment and rotational excitation; y_k and M_k are the mole fraction and mass of the k th species, respectively, m is the electron mass, and T_g is the gas temperature; $\sigma_{mk}(\epsilon)$ and $\sigma_{jk}(\epsilon)$ are the cross sections for momentum transfer and inelastic collision j between electrons and the k th species, and I_{jk} is the energy threshold for inelastic collision j between electrons and the k th species.

The contributions from dissociative, electronic, and vibrational excitation and ionization processes are given in the first term of Eq. (5). The contribution from the two-body and three-body attachment processes is given as follows:

$$Q_{att}(f) = -\left(\frac{2}{m}\right)^{1/2} \left(\sum_k y_k \sigma_{att,k}(\epsilon) \right) \epsilon f(\epsilon, t), \quad (6)$$

where $\sigma_{att,k}(\epsilon)$ is the attachment cross section. The continuous approximation^{4,8} was used for $Q_{rot}(f)$,

$$Q_{rot}(f) = 4 \left(\frac{2}{m}\right)^{1/2} B_0 y_M \sigma_{rot}(\epsilon) \frac{\partial}{\partial \epsilon} [\epsilon f(\epsilon, t)], \quad (7)$$

where B_0 is the rotational constant and $\sigma_{rot}(\epsilon)$ is the rotational excitation cross section, and y_M is the mole fraction of the molecular species.

2. Boundary and initial conditions

The boundary conditions for Eq. (2) are written in the form

$$J_\epsilon = N \sum_k y_k \langle \sigma_{i,k}(\epsilon) v \rangle, \quad \text{at } \epsilon = 0, \quad \forall t, \quad (8)$$

$$f \rightarrow 0 \quad \text{as } \epsilon \rightarrow \infty, \quad \forall t, \quad (9)$$

where J_ϵ is the flux defined by Eq. (3) and $\langle \sigma_{i,k}(\epsilon) v \rangle$ is the velocity-averaged ionization rate coefficient for species k . Equation (8) denotes that the newly appearing electrons flow into the energy domain through the boundary $\epsilon = 0$.^{18,25}

The initial EEDF was chosen as Maxwellian with temperature T_e ,

$$f(\epsilon) = (2/\sqrt{\pi}) \exp(-\epsilon/kT_e)/(kT_e)^{3/2} \quad \text{at } t=0, \quad (10)$$

with a mean electron energy $\langle \epsilon \rangle = \frac{3}{2} kT_e$.

In addition, the EEDF was normalized by

$$\int_0^\infty \sqrt{\epsilon} f(\epsilon) d\epsilon = 1. \quad (11)$$

3. Applied electric field

Both direct current (dc) and alternating current (ac) fields were used in Eq. (2),

$$\text{for dc case:} \quad E = E_0, \quad (12)$$

$$\text{for ac case:} \quad E = E_0 \sin \omega t, \quad (13)$$

where E_0 is the amplitude and ω is the angular frequency of the electric field. The effective dc field is defined as

$$E_{\text{eff}} = \frac{E_0/\sqrt{2}}{\sqrt{(\omega/\nu_m)^2 + 1}}. \quad (14)$$

In the present work the energy dependence of the momentum exchange frequency ν_m was retained. Frequencies used in the calculation were $\omega/2\pi = 1, 10, 13.56,$ and 100 MHz.

4. Electron transport and reaction coefficients

Once the EEDF is found, a number of electron swarm parameters can be calculated. The mean electron energy and rate coefficients of electron-particle reactions were computed by using Eqs. (15) and (16), respectively:

$$\langle \epsilon \rangle = \int_0^\infty f(\epsilon) \epsilon^{3/2} d\epsilon, \quad (15)$$

$$k_j = \left(\frac{2}{m}\right)^{1/2} \int_0^\infty \sigma_j(\epsilon) f(\epsilon) \epsilon d\epsilon, \quad (16)$$

where j stands for the j th inelastic process with cross section $\sigma_j(\epsilon)$. The electron drift velocity v_d and the diffusion coefficient D_e were calculated as follows:

$$v_d = -\frac{1}{3} \left(\frac{2}{m}\right)^{1/2} \left(\frac{eE}{N}\right) \int_0^\infty \frac{\epsilon}{\sum_k y_k \sigma_{mk}(\epsilon)} \frac{\partial f(\epsilon)}{\partial \epsilon} d\epsilon, \quad (17)$$

$$D_e = \frac{1}{3N} \left(\frac{2}{m}\right)^{1/2} \int_0^\infty \frac{f(\epsilon)}{\sum_k y_k \sigma_{mk}(\epsilon)} d\epsilon. \quad (18)$$

Then, the electron mobility μ_e , characteristic energy ϵ_k , effective momentum exchange frequency $\nu_{m,\text{eff}}$, and energy relaxation frequency ν_u were obtained as

$$\mu_e = v_d/E, \quad (19)$$

$$\epsilon_k = D_e/\mu_e, \quad (20)$$

$$v_{m,\text{eff}}/N = (1/mv_d)(eE/N), \quad (21)$$

$$v_d/N = v_d(eE/N)/(\epsilon_k - kT_g). \quad (22)$$

Swarm parameters were calculated for a typical gas number density $N = 3 \times 10^{16} \text{ cm}^{-3}$, which is equivalent to 1 Torr at 322 K.

B. Method of solution

The finite-element method^{26,27} was employed to solve the time-dependent Boltzmann equation [Eq. (2)]. A special weighting function was defined to account for the contribution of the element containing $(\epsilon + I_{jk})$ to the element containing ϵ . The equation was solved by a predictor/multicorrector algorithm associated with the Crank-Nicholson scheme. The EEDF was normalized at every time step to eliminate errors accumulated in the process of numerical integration.¹⁸ A nonuniform energy mesh and a uniform time step were used. Solutions were obtained between $\epsilon = 0$ and $\epsilon = \epsilon_{\text{max}}$, where ϵ_{max} is large enough such that $f(\epsilon_{\text{max}}) \rightarrow 0$. A finer mesh was used where the collision cross sections have sharp changes. The convergence to steady state (or periodic steady state) was detected by the following criteria:

for dc case:

$$\xi_{\text{ss,dc}} = \left(\sum_{i=1}^{\text{NP}} [f(\epsilon_i, t + \Delta t) - f(\epsilon_i, t)]^2 \right)^{1/2} (\text{NP})^{-1}, \quad (23)$$

for ac case:

$$\xi_{\text{ss,ac}} = \left\{ \sum_{j=1}^{\text{NT}} \left[\left(\frac{k_{x,j}}{k_{x,\text{avg}}} \right)_{(I+1)\tau} - \left(\frac{k_{x,j}}{k_{x,\text{avg}}} \right)_{I\tau} \right]^2 \right\}^{1/2} (\text{NT})^{-1}, \quad (24)$$

where $f(\epsilon_i, t)$ is the EEDF at energy ϵ_i and time t , k_x is the rate coefficient of an inelastic process which is sensitive to the tail of the EEDF (this was taken to be ionization), $k_{x,j}$ is the value of k_x at time t_j , and $k_{x,\text{avg}}$ is the time-average value of $k_{x,j}$ over a period of the applied field. NP is the number of nodal points in the energy coordinate, NT is the number of time steps per rf cycle (typically a few 100), $\xi_{\text{ss,dc}}$ and $\xi_{\text{ss,ac}}$ are user-specified error tolerances (typically 10^{-6}).

III. CROSS SECTIONS

A. Oxygen

For this system only electron collisions with molecular oxygen were considered, i.e., the concentration of atomic oxygen was assumed negligibly small. Various kinds of inelastic processes such as excitation, ionization, and attachment, play an important role. Some of the excited states are potentially important sources of stored energy, e.g., the oxygen molecules in the lowest metastable state $a^1\Delta_g$.²⁸ Dissociative excitation (130 nm line) with a threshold of 14.7 eV, and electronic excitations to singlet delta ($a^1\Delta$, 0.977 eV loss), singlet sigma ($b^1\Sigma$, 1.627 eV loss) as well as excitations with 4.5, 6.0, 8.4, and 9.97 eV loss were included. In molecular gas discharges vibrational excitation plays an important role at intermediate values of E/N .

TABLE I. Important inelastic electron collision processes in oxygen.

Process		Threshold (eV)
Dissociative excitation	$\text{O}_2 + e^- \rightarrow \text{O}_2^* + e^- \rightarrow 2\text{O} + e^-$	14.7
Electronic excitations	$\text{O}_2 + e^- \rightarrow \text{O}_2^* + e^-$	
$a^1\Delta$		0.977
$b^1\Sigma$		1.627
4.5 eV loss		4.5
6.0 eV loss		6.0
8.4 eV loss		8.4
9.97 eV loss		9.97
Vibrational excitations	$\text{O}_2 + e^- \rightarrow \text{O}_2^* + e^-$	
$v=1$		0.19
$v=2$		0.38
$v=3$		0.57
$v=4$		0.75
Rotational excitation	$\text{O}_2 + e^- \rightarrow \text{O}_2^* + e^-$	0.02
Molecular ionization	$\text{O}_2 + e^- \rightarrow \text{O}_2^+ + 2e^-$	12.06
Dissociative ionization	$\text{O}_2 + e^- \rightarrow \text{O}^+ + \text{O} + 2e^-$	
Two-body attachment	$\text{O}_2 + e^- \rightarrow \text{O}^- + \text{O}$	0.0
Three-body attachment	$\text{O}_2 + \text{O}_2 + e^- \rightarrow \text{O}_2^- + \text{O}_2$	0.0

For oxygen, four vibrational modes ($v=1, 2, 3,$ and 4) with energy loss of 0.19, 0.38, 0.57, and 0.75 eV were considered. Rotational excitation was also included, as well as ionization with energy loss of 12.06 eV. Also, electrons can be captured by molecules to form negative ions. Both two-body and three-body attachment were included. A summary of the processes considered is shown in Table I. The tabulated collision cross sections of Phelps²⁹ were employed. The rotational constant B_0 for O_2 is 1.7×10^{-4} eV.³⁰

B. Chlorine

For the chlorine discharge, electron collisions with both atomic and molecular chlorine were taken into account. The purpose was to investigate the effect of gas composition on the electron transport and reaction coefficients. The inelastic processes included in the calculation are listed in Table II. The same collision cross sections as before were used.^{11-13,31}

IV. RESULTS AND DISCUSSION

A. Oxygen

Before any further calculations, the finite-element code was "tuned" and the numerical results were checked against known data. Numerical experiments were performed to determine the optimum mesh and time-step sizes. It was also verified that the steady state is independent of the initial condition.

The EEDF for a dc field with different E/N values is given in Fig. 1. The EEDF is non-Maxwellian in the range $E/N = 10-250$ Td. The tail of the EEDF falls off rapidly as the high-energy electrons are depleted via various inelastic collisions. The mean electron energy increases with E/N . The electron swarm parameters were found to be in good agreement with the results of Phelps.²⁹ A detailed compar-

TABLE II. Important inelastic electron collision processes in chlorine.

Process		Threshold (eV)
Dissociative excitation	$\text{Cl}_2 + e^- \rightarrow \text{Cl}_2^*(C^1\Pi) + e^- \rightarrow 2\text{Cl} + e^-$	3.12
Electronic excitations (molecular)	$\text{Cl}_2 + e^- \rightarrow \text{Cl}_2^* + e^-$	
	$B^3\Pi$	2.49
	$2^1\Pi$ and $2^1\Sigma$	9.25
Electronic excitations (atomic)	$\text{Cl} + e^- \rightarrow \text{Cl}^* + e^-$	
	$4s$	8.9
	$4p$	10.4
	$3d$	10.9
	$5p$	11.8
	$4d$	12.0
	$5d$	12.4
Vibrational excitation	$\text{Cl}_2 + e^- \rightarrow \text{Cl}_2^* + e^-$	0.0689
Molecular ionization	$\text{Cl}_2 + e^- \rightarrow \text{Cl}_2^+ + 2e^-$	11.47
Atomic ionization	$\text{Cl} + e^- \rightarrow \text{Cl}^+ + 2e^-$	12.99
Dissociative attachment	$\text{Cl}_2 + e^- \rightarrow \text{Cl}_2^- \rightarrow \text{Cl}^- + \text{Cl}$	0.0

ison showed that deviations never exceeded 3.0%. This confirms that the finite-element method can be employed to solve the Boltzmann equation and the modified weighting function approach is proper.

Figure 2 shows the mean electron energy $\langle \epsilon \rangle$ and dissociative excitation rate coefficient k_d as a function of E/N for a dc field. k_d is important in etching discharges that are based on the action of oxygen atoms, e.g., etching of polymer films.³² The characteristic electron energy ϵ_k is also shown. The lines are the result of the finite-element calculation, and the data points are taken from Phelps.²⁹ This again verifies the correctness of the finite-element calculation. The chain curve shown in Fig. 2 is the dissociative excitation rate coefficient k_{dM} calculated assuming a Maxwellian distribution with a mean energy equal to that of the actual distribution. One observes significant differences between k_d and k_{dM} , especially at low values of E/N .

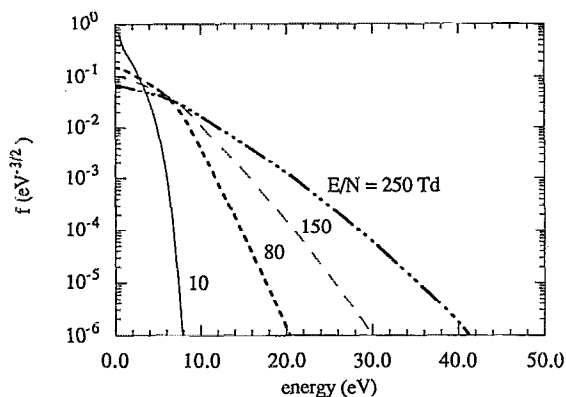


FIG. 1. Steady-state electron energy distribution function for O_2 dc fields of $E/N=10, 80, 150,$ and 250 Td.

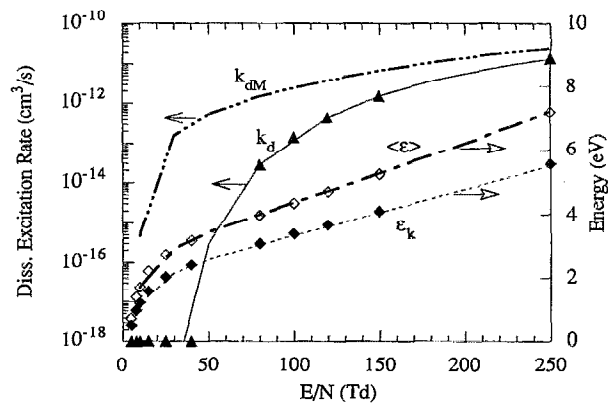


FIG. 2. Steady-state values of dissociative excitation rate coefficient k_d , mean electron energy $\langle \epsilon \rangle$, and characteristic energy ϵ_k , as a function of E/N for a dc field in O_2 . Phelps' results are shown as points. k_{dM} is calculated assuming a Maxwellian distribution with the same mean electron energy as the actual distribution.

The time evolution of the electron transport and reaction coefficients in oxygen under a step change in the applied dc field is analyzed next. Figure 3 displays the time dependence of several swarm parameters when a dc field of $E/N=80$ Td is imposed at time $t=0$. The initial distribution was assumed Maxwellian with mean electron energy 1.5 eV (dashed lines) and 15 eV (solid lines). The steady-state values of the swarm parameters are not affected by the choice of initial condition, albeit the transient behavior is considerably different.³²

Figure 4 shows the time-dependent behavior of some electron swarm parameters for a dc field of $E/N=80$ Td applied at $t=0$, for two different oxygen number densities. The initial distribution was assumed Maxwellian with mean energy 1.5 eV. Although the transient behavior varies with either the electric-field strength or the gas density, the steady-state results are a function of the reduced electric field strength E/N only. The steady state is reached faster for higher gas number density N as the number of collisions is proportional to N . The transient lasts for < 10 ns under these conditions.

Figure 5 shows the decay of several swarm parameters. The EEDF was first allowed to reach steady state with a dc electric field of $E/N=80$ Td. The field was then switched off at time $t=2$ ns (the switch-off time is of no consequence here). The excitation and ionization rate coefficients, both of which are tail processes, decay to very small values within several nanoseconds after field extinction. The mean energy, however, decreases at a much slower rate. The mean energy is determined primarily by the low-energy electrons. Hence, processes with low threshold energy such as attachment and vibrational excitation will continue long after excitation and ionization have extinguished. Of course, one must also consider the decay of the electron density n_e since the rate of any electron-impact process depends on n_e as well. The decay and buildup of the EEDF is of importance in pulsed plasmas. Significantly different chemistry can happen in the "afterglow" as compared to the "active" discharge.³³

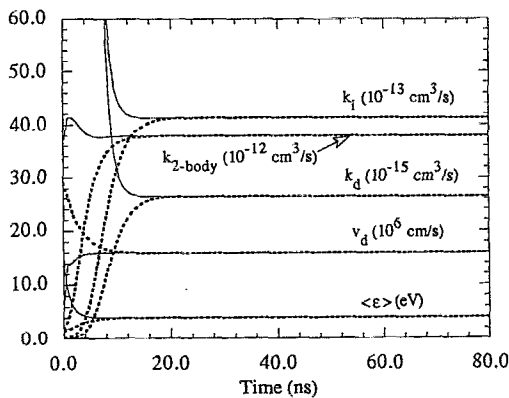


FIG. 3. Time evolution of electron swarm parameters in O_2 for a dc field of $E/N=80$ Td applied at $t=0$. Solid and dashed curves correspond to initial mean electron energy of 15 and 1.5 eV, respectively. The initial distribution function was a Maxwellian.

The time-dependent EEDF for a sinusoidal field with peak $E/N=80$ Td and a frequency of 1 MHz is shown in Fig. 6(a). The EEDF is modulated strongly at this low frequency. The tail of the distribution extends to higher energies when the applied field has a high value (e.g., at $\omega t=\pi/2$ and $3\pi/2$), and retracts to lower energies when the applied field is low ($\omega t=0, \pi$, and 2π). The EEDFs are identical for $\omega t=0$ and π , or $\omega t=\pi/4$ and $5\pi/4$. This implies that the EEDF is modulated at twice the applied field frequency.

A magnification of the EEDF in the low-energy region is shown in Fig. 6(b). The spikes in the EEDF near the zero crossings of the applied field ($\omega t=0, \pi$) are caused by the vibrational excitations which have very sharp resonant-type cross sections at these low energies.

Figures 7(b), 7(c), and 7(d) show the time behavior of the mean and characteristic electron energy, dissociative excitation rate coefficient, and ionization rate coefficient, respectively, under the same conditions as for Fig. 6. The applied electric field is plotted in Fig. 7(a). The excitation and ionization rate coefficients are modulated fully, but the

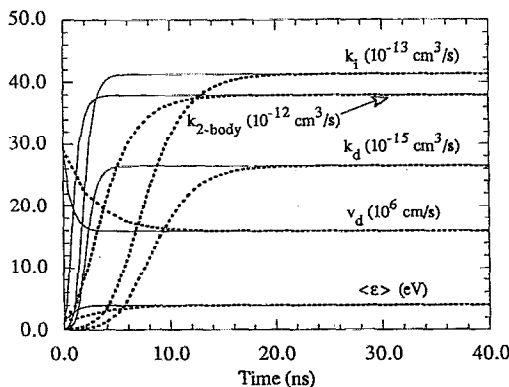


FIG. 4. Time evolution of electron swarm parameters in O_2 for a dc field of $E/N=80$ Td applied at $t=0$. Solid and dashed curves correspond to oxygen number density of 1.2×10^{17} and $3 \times 10^{16} \text{ cm}^{-3}$, respectively.

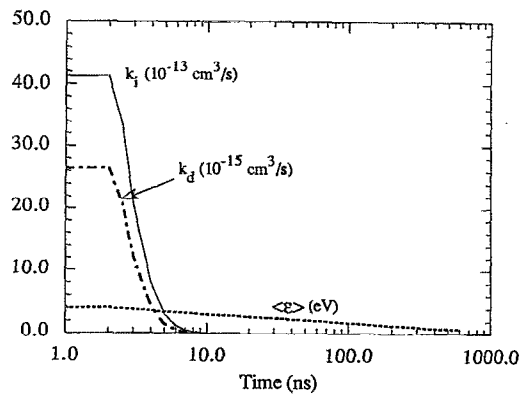


FIG. 5. Decay of electron swarm parameters in O_2 . The electron energy distribution function was first allowed to reach steady state under a dc field of $E/N=80$ Td. Then, at $t=2$ ns the field was switched off.

mean electron energy is not. In addition, a slight phase shift is observed in the mean (and characteristic) energy. This can be explained as follows: since high-energy (tail) electrons have more channels for losing their energy than low-energy electrons, the tail of the EEDF is modulated much more than the low-energy region (see also Fig. 6). Now, ionization and excitation are tail processes, whereas the mean energy is determined primarily by the more pop-

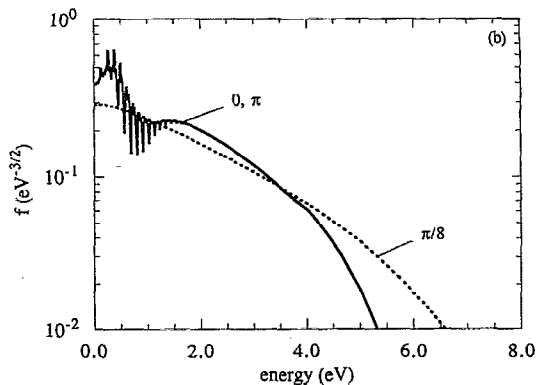
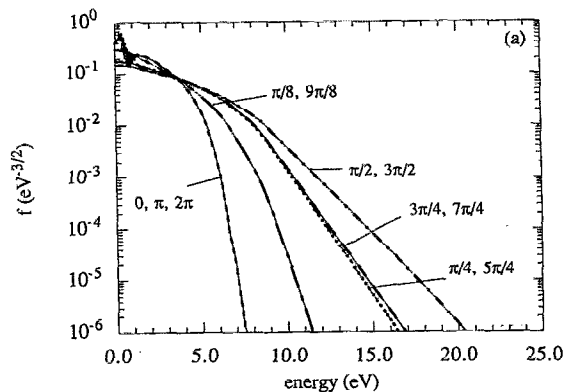


FIG. 6. (a) Time-dependent electron energy distribution function $f(\epsilon, t)$ in O_2 after periodic steady state has been reached. An ac field with frequency of 1 MHz and peak $E/N=80$ Td was applied. (b) An expanded view of the low-energy region for $\omega t=0, \pi$, and $\pi/8$.

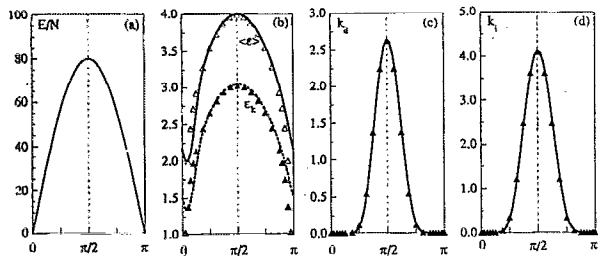


FIG. 7. Time-dependent swarm parameters under the conditions of Fig. 6. (a) applied electric field (Td); (b) mean $\langle \epsilon \rangle$ and characteristic electron energy ϵ_k (eV); (c) dissociative excitation rate coefficient k_d (10^{-14} cm³/s); and (d) ionization rate coefficient k_i (10^{-12} cm³/s). Points are calculated using the QSS approximation.

ulous low-energy electrons. In other words, the energy relaxation frequency for the tail electrons is much higher than the applied frequency, but this is not so for the low-energy electrons. The points superimposed on the curves of Figs. 7(b)–7(d) correspond to the QSS approximation. One observes that this approximation is excellent for calculating electron reaction rate coefficients at a frequency of 1 MHz.

Figure 8 shows the time-dependent EEDF for a peak $E/N=80$ Td and a frequency of 100 MHz. The degree of modulation is much reduced compared to the 1 MHz case (Fig. 6). Significant modulation of the tail of the EEDF still persists, but the bulk of the distribution is only slightly modulated. Furthermore, no spikes are observed at low energy near the zero crossings of the field. A phase shift between the applied field and the EEDF is clearly evident since the tail at $\omega t=0$ extends further than that at $\omega t=\pi/4$. As the frequency is increased even further, modulation of the whole distribution will cease and a time-independent EEDF will be obtained. This is expected to happen for frequencies $\omega/2\pi > 1$ GHz. In this high-frequency regime the quasi-steady-state assumption for f_1 breaks down. One then needs to solve a coupled system of time-dependent equations for f_0 and f_1 .

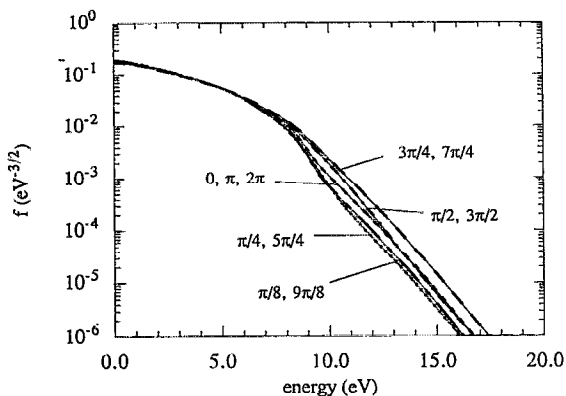


FIG. 8. Time-dependent electron energy distribution function $f(\epsilon, t)$ in O_2 after periodic steady state has been reached. An ac field with frequency of 100 MHz and peak $E/N=80$ Td was applied.

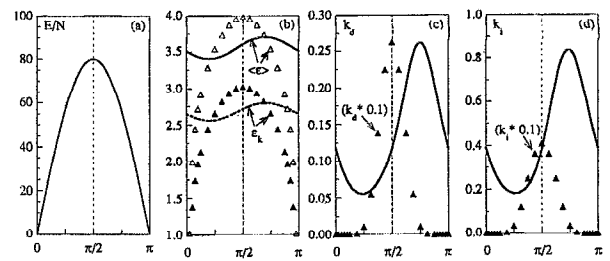


FIG. 9. Time-dependent swarm parameters under the conditions of Fig. 8. (a) applied electric field (Td); (b) mean $\langle \epsilon \rangle$ and characteristic electron energy ϵ_k (eV); (c) dissociative excitation rate coefficient k_d (10^{-14} cm³/s); and (d) ionization rate coefficient k_i (10^{-12} cm³/s). Points are calculated using the QSS approximation. Points for k_d and k_i are plotted after reducing by ten times.

Figures 9(b), 9(c), and 9(d) show the time behavior of the mean and characteristic electron energy, dissociative excitation rate coefficient, and ionization rate coefficient, respectively, under the same conditions as for Fig. 8. The applied electric field is plotted in Fig. 9(a). In contrast to Fig. 7, the excitation and ionization rate coefficients are not modulated fully. Modulation of the mean and characteristic energies is even weaker. In addition, a large phase shift is observed between the applied field and the swarm parameters. The points superimposed on the curves of Figs. 9(b)–9(d) correspond to the QSS approximation. It is apparent that this approximation is not valid for 100 MHz.

B. Chlorine

Figure 10 shows the modulation of the EEDF for a peak reduced field of $E/N=200$ Td and a frequency of 10 MHz, for 100% Cl_2 gas. The distribution function is modulated strongly. The electron mean energy, dissociative excitation rate coefficient, and total (molecular plus atomic chlorine) ionization rate coefficient are shown in Figs. 11(b), 11(c), and 11(d), respectively. The applied field is shown in Fig. 11(a). Results in Fig. 11 were calculated for three different atomic chlorine mole fractions, 0%, 50%, and 100%, the balance being molecular chlorine. For a constant applied field, the mean energy and rate coefficients increase with increasing mole fraction of atomic chlorine y_{Cl} . The opposite is true at microwave frequencies, i.e., the mean energy and rate coefficients decrease with increasing y_{Cl} . This has been explained before.¹³

Figures 12(b), 12(c), 12(d), and 12(e) show the time behavior of the mean and characteristic electron energy, dissociative excitation, ionization, and attachment rate coefficients, respectively, for a peak $E/N=200$ Td and a frequency of 13.56 MHz. The applied electric field is plotted in Fig. 12(a). The excitation and ionization rate coefficients are modulated fully, but the mean and characteristic energy as well as the attachment rate coefficient are not. In addition, a slight phase shift is observed in the swarm parameters. The points superimposed on the curves of Figs. 12(b)–12(e) were calculated for a dc electric field of magnitude equal to that of the actual ac field at the particular instant in time (QSS approximation). One observes that

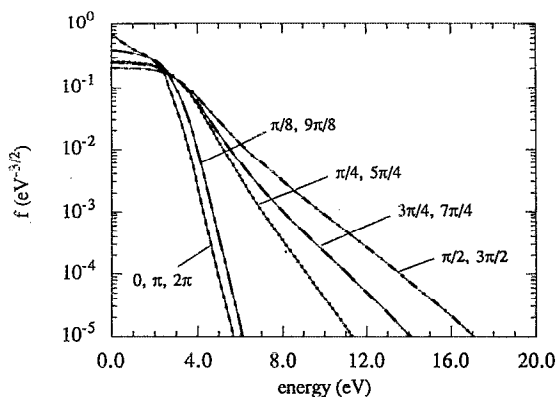


FIG. 10. Time-dependent electron energy distribution function $f(\epsilon, t)$ in 100% Cl_2 after periodic steady state has been reached. An ac field with frequency of 10 MHz and peak $E/N=200$ Td was applied.

the system follows the QSS approximation quite well at a frequency of 13.56 MHz. This approximation was made to conserve computation time when modeling a parallel-plate plasma reactor.¹¹ As shown below (Table IV), the QSS approximation is excellent for calculating radical production rates in the bulk region of a chlorine discharge at 13.56 MHz and ~ 1 Torr. The QSS approximation is also valid when the electric field is increased to 500 Td (Fig. 13). Higher electric fields are found near the walls of the discharge (sheath). However, one needs to solve the space- and time-dependent Boltzmann equation to account for steep gradients in the electric fields in the sheath region.

C. Comparison with approximate solutions

In plasma reactor modeling one is frequently interested in calculating the production rate of radicals and ions. For frequencies in the MHz range, these species do not respond to the rapid variation of the field, and time-average dissociation k_d and ionization k_i rate coefficients may be appropriate. Table III lists a comparison of swarm parameters in oxygen calculated by three methods: (a) the time-dependent swarm parameter was found for the actual ac

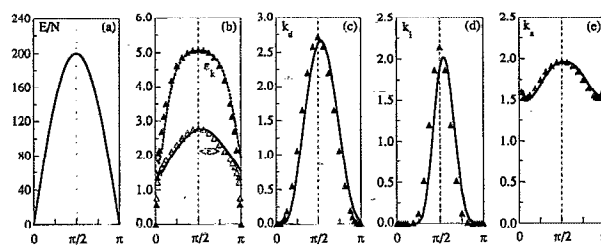


FIG. 12. Time-dependent swarm parameters for 100% Cl_2 . An ac field with frequency of 13.56 MHz and peak $E/N=200$ Td was applied; (a) applied electric field (Td); (b) mean $\langle \epsilon \rangle$ and characteristic electron energy ϵ_k (eV); (c) dissociative excitation rate coefficient k_d (10^{-9} cm^3/s); (d) ionization rate coefficient k_i (10^{-11} cm^3/s), and (e) dissociative attachment rate coefficient (10^{-10} cm^3/s). Points are calculated using the QSS approximation.

field and then it was time averaged (this is shown as ac); (b) the parameter was found assuming that the EEDF follows completely the applied ac field and then it was time averaged (shown as QSS); and (c) the parameter was found using the effective dc field (shown as Eff. dc). For a frequency < 10 MHz the QSS approximation is very reasonable for oxygen. The effective dc approximation is not good for < 10 MHz, but for 100 MHz it is within 30% of the time-averaged ac value, for the conditions studied. Although the effective electric-field strengths for 1, 10, and 100 MHz are almost the same (within 3%), the time-averaged ac swarm parameters are quite different. Table IV shows the corresponding comparison for 100% Cl_2 at 13.56 MHz. The QSS approximation is excellent, but the effective dc approximation is inadequate. The QSS approximation gives radical production and ionization rate coefficients within 1% and 5%, respectively, of the actual value. As mentioned earlier, use of the QSS approximation reduces substantially the computation time in plasma reactor modeling. In essence, one can then solve the time-independent Boltzmann equation for different values of E/N , and generate look-up tables or analytic expressions of the electron swarm parameters as function of E/N and gas composition. Balance equations determining the self-consistent electric field and electron and radical densities

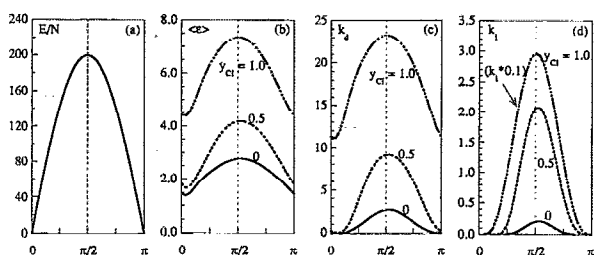


FIG. 11. Time-dependent swarm parameters as a function of atomic chlorine mole fraction y_{Cl} (balance is molecular chlorine). An ac field with frequency of 10 MHz and peak $E/N=200$ Td was applied: (a) applied electric field (Td); (b) mean electron energy $\langle \epsilon \rangle$ (eV); (c) dissociative excitation rate coefficient k_d (10^{-9} cm^3/s); (d) total ionization rate coefficient k_i (10^{-10} cm^3/s). For the case $y_{\text{Cl}}=1$, k_i is plotted after reducing by ten times.

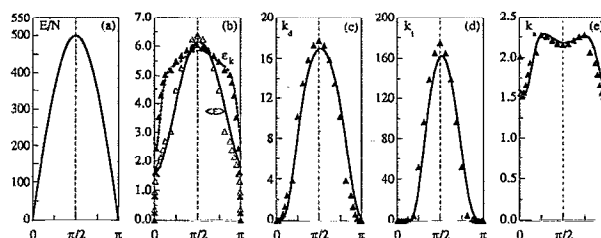


FIG. 13. Time-dependent swarm parameters for 100% Cl_2 . An ac field with frequency of 13.56 MHz and peak $E/N=500$ Td was applied; (a) applied electric field (Td); (b) mean $\langle \epsilon \rangle$ and characteristic electron energy ϵ_k (eV); (c) dissociative excitation rate coefficient k_d (10^{-9} cm^3/s); (d) ionization rate coefficient k_i (10^{-11} cm^3/s), and (e) dissociative attachment rate coefficient (10^{-10} cm^3/s). Points are calculated using the QSS approximation.

TABLE III. Mean electron energy, dissociative excitation, and ionization rate coefficients in O₂. Comparison of time-average values for ac field (peak $E/N=80$ Td) with the quasi-steady-state (QSS) and effective dc field approximations.

	$\langle \epsilon \rangle$ (eV)	k_d (cm ³ /s)	k_i (cm ³ /s)
ac, 1 MHz	3.336	7.059×10^{-15}	1.231×10^{-12}
Eff. dc	3.540	1.109×10^{-15}	3.616×10^{-13}
QSS	3.207	6.996×10^{-15}	1.221×10^{-12}
ac, 10 MHz	3.454	6.418×10^{-15}	1.144×10^{-12}
Eff. dc	3.539	1.108×10^{-15}	3.611×10^{-13}
QSS	3.207	6.996×10^{-15}	1.221×10^{-12}
ac, 100 MHz	3.555	1.374×10^{-15}	4.482×10^{-13}
Eff. dc	3.452	9.599×10^{-16}	3.174×10^{-13}
QSS	3.207	6.996×10^{-15}	1.221×10^{-12}

can then be integrated directly (and rapidly). This procedure obviates the need of solving the time-dependent Boltzmann equation coupled with the other balance equations.

V. SUMMARY

The spatially uniform time-dependent Boltzmann equation was solved to determine the electron energy distribution function (EEDF) in oxygen and chlorine gases. A general finite-element code was developed which is applicable to any gas mixture. The time evolution of the EEDF and of the electron swarm parameters under step changes of a dc electric field or under a radio-frequency ac field was examined.

For electric fields found in the bulk plasma of glow discharge reactors at ~ 1 Torr, the effective dc approximation is not applicable for oxygen and chlorine gases for frequencies < 10 MHz. The quasi-steady-state approximation is excellent for chlorine at < 13.56 MHz, giving dissociation and ionization rate coefficients within a few % of the actual value. By making this approximation one can reduce substantially the computation time needed for modeling these discharges.

TABLE IV. Dissociative excitation and ionization rate coefficients in Cl₂. Comparison of time-average values for 13.56 MHz ac field (peak $E/N=200$ and 500 Td) with the quasi-steady-state (QSS) and effective dc field approximations.

		200 Td	500 Td
k_d (cm ³ /s)	ac	1.191×10^{-9}	9.067×10^{-9}
	Eff. dc	1.062×10^{-9}	1.018×10^{-8}
	QSS	1.198×10^{-9}	8.996×10^{-9}
k_i (cm ³ /s)	ac	5.682×10^{-12}	6.522×10^{-10}
	Eff. dc	1.206×10^{-12}	5.160×10^{-10}
	QSS	5.967×10^{-12}	6.824×10^{-10}

The finite-element code can also handle spatial dependencies of the EEDF. Spatiotemporal solutions of the EEDF are useful in large scale simulations of glow discharge plasmas.

ACKNOWLEDGMENTS

We thank Dr. Y.-O. Park of Pusan National University of Technology (Korea) for helpful discussions concerning the finite-element solution of the Boltzmann equation. Financial support from the State of Texas through the Texas Advanced Research Program and from the Welch Foundation is gratefully acknowledged. We also thank the Pittsburgh Supercomputer Center (supported by NSF) for a supercomputer time grant.

- L. Kline and M. J. Kushner, *Crit. Rev. Solid State Mater. Sci.* **16**, 1 (1989).
- B. E. Cherrington, *Gaseous Electronics and Gas Lasers* (Pergamon, New York, 1979).
- W. L. Morgan and B. M. Penetrante, *Comput. Phys. Commun.* **58**, 127 (1990).
- A. G. Engelhardt and A. V. Phelps, *Phys. Rev.* **131**, 2115 (1963).
- W. L. Nighan, *Phys. Rev. A* **2**, 1989 (1970).
- H. Tagashira, Y. Sakai, and S. Sakamoto, *J. Phys. D* **10**, 1051 (1977).
- S. Yachi, Y. Kitamura, K. Kitamori, and H. Tagashira, *J. Phys. D* **21**, 914 (1988).
- S. C. Brown, *Hand. Phys.* **22**, 531 (1956); P. E. Luft, JILA Information Center, Report No. 14, 1975.
- C. M. Ferreira and J. Loureiro, *J. Phys. D* **16**, 2471 (1983).
- L. L. Alves and C. M. Ferreira, *J. Phys. D* **24**, 581 (1991).
- E. S. Aydil and D. J. Economou, *J. Electrochem. Soc.* **139**, 1396 (1992).
- E. S. Aydil and D. J. Economou, *J. Electrochem. Soc.* **139**, 1406 (1992).
- S. Deshmukh and D. J. Economou, *J. Appl. Phys.* **72**, 4597 (1992).
- K. Ohe and T. Kimura, *Jpn. J. Appl. Phys.* **28**, 1997 (1989).
- D. N. Ruzic and J. L. Wilson, *J. Vac. Sci. Technol. A* **8**, 3746 (1990).
- T. Makabe and N. Goto, *J. Phys. D* **21**, 887 (1988).
- M. Capitelli, C. Gorse, R. Winkler, and J. Wilhelm, *Plasma Chem. Plasma Process* **8**, 399 (1988); R. Winkler, M. Dilonardo, M. Capitelli, and J. Wilhelm, *Plasma Chem. Plasma Process* **7**, 125 (1987); **7**, 245 (1987).
- V. A. Feoktistov, A. M. Popov, O. B. Popovicheva, A. T. Rakhimov, T. V. Rakhimova, and E. A. Volkova, *IEEE Trans. Plasma Sci.* **PS-19**, 163 (1991).
- L. J. Overzet, J. H. Beberman, and J. T. Verdeyen, *J. Appl. Phys.* **66**, 1622 (1989); Y. Watanabe, M. Shiratani, and H. Makino, *Appl. Phys. Lett.* **57**, 1616 (1990).
- A. Bouchoule, A. Plain, L. Boufendi, J. Ph. Blondau, and C. Laure, *J. Appl. Phys.* **70**, 1991 (1991); S. G. Hansen, G. Luckman, and S. Colson, *Appl. Phys. Lett.* **53**, 1588 (1988).
- P. J. Drallos and J. M. Wadehra, *Phys. Rev. A* **40**, 1967 (1989); P. J. Drallos and J. M. Wadehra, *J. Appl. Phys.* **63**, 5601 (1988).
- R. Winkler, H. Deutsch, J. Wilhelm, and Ch. Wilke, *Beitr. Plasmaphys.* **24**, 285 (1984); **24**, 303 (1984).
- L. C. Pitchford and A. V. Phelps, *Phys. Rev. A* **25**, 540 (1982); K. Kitamori, H. Tagashira, and Y. Sakai, *J. Phys. D* **11**, 283 (1978); H. Brunet and P. Vincent, *J. Appl. Phys.* **50**, 4700 (1979); **50**, 4708 (1979); E. Riehley, *ibid.* **71**, 4190 (1992).
- S.-K. Park and D. J. Economou, *J. Appl. Phys.* **68**, 3904 (1990).
- S. D. Rockwood, *Phys. Rev. A* **8**, 2348 (1973).
- L. Lapidus and W. E. Schiessler, *Numerical Methods for Differential Systems* (Academic, New York, 1976).
- T. J. R. Hughes, *The Finite Element Method* (Prentice-Hall, Englewood Cliffs, NJ, 1987).
- C. Yamabe and A. V. Phelps, *J. Chem. Phys.* **78**, 2984 (1983).
- A. V. Phelps, JILA Information Center, Report No. 28, 1985.
- H. Myers, *J. Phys. B* **2**, 393 (1969).

- ³¹G. L. Rogoff, J. M. Kramer, and R. B. Piejak, *IEEE Trans. Plasma Sci.* **PS-14**, 103 (1986).
- ³²S.-K. Park and D. J. Economou, *J. Appl. Phys.* **66**, 3256 (1989).
- ³³L. J. Overzet and L. Luo, in *Proceedings of the 9th Plasma Processing*

Symposium, edited by G. S. Mathad and D. W. Hess (Electrochemical Society, New York, 1992), Vol. 92-18, p. 64; L. J. Overzet, Abstract No. 442, presented at the 39th AVS National Symposium, Chicago, Illinois, November 9-13, 1992.